J. Appl. Cryst. (1993). **26**, 122–127

Study of Brazil Twin Boundaries in Synthetic Quartz by means of Simulations of X-ray Topographs

BY M. GONZÁLEZ-MAÑAS AND M. A. CABALLERO

Departamento de Estructura y Propriedades de los Materiales, Facultad de Ciencias, Universidad de Cádiz, Apdo 40, *Puerto Real* 11510, *Cádiz, Spain*

AND B. CAPELLE AND Y. EPELBOIN

Laboratoire de Minéralogie-Cristallographie, UA 009 *CNRS, Universités P. et M. Curie et Paris* VII, *BP* 115, 75252 *Paris CEDEX* 05, *France*

(*Received* 14 *March* 1992; *accepted* 4 *September* 1992)

Abstract

$(0\bar{1}11)$ twin boundaries of *Y*-cut synthetically-grown quartz crystals are studied by means of X-ray section topographs. The images show an anomalous contrast and no extinction condition can be found. Simulated images demonstrate that the twin boundaries are not simple planar defects. They may be described as lamellae of a non-diffracting material. Their thickness is of the order of 15 μm and, within these boundaries, the Fourier components of the dielectric susceptibility are drastically reduced by one order of magnitude.

1. Introduction

González-Mañas & Caballero (1991) have previously studied the generation of Brazil twins in $-X$ and Z' growth sectors of *Y*-bar synthetic quartz crystals. They have also described the associated defects and their evolution during the growth. Brazil twin domains have been clearly identified by their boundary contrast in X-ray topographs. Two kinds of boundaries have been reported.

(*a*) Some boundaries are parallel to the major rhombohedron plane $(0\bar{1}11)$, extending across the $-X$ and Z' growth sectors. Their orientation does not change during the entire growth process.

(*b*) Others, restrained to the Z' growth sector, are irregular. At the beginning of the growth, near the seed, they are parallel to the crystallographic $\{10\bar{1}0\}$ planes, then they change progressively and become stepped non-crystallographic boundaries. They are predominant in the largest Brazil twins. The Brazil twin domain, in the $-X$ growth sector, is mainly made of two trapezohedral $(6\bar{5}1\bar{1})$ and $(6\bar{5}\bar{1}1)$ growth subsectors. Other growth subsectors always appear in the $-X$ growth sector (Fig. 1): two trapezohedral sectors, $(\bar{6}15\bar{1})$ and $(\bar{6}51\bar{1})$, as a result of the twin symmetry and two rhombohedral sectors, $(\bar{3}0\bar{3}1)$ and $(\bar{3}301)$. These growth subsectors, including those of the twin domain, constitute the twofold symmetry polyhedra observed on the $-X$ surfaces.

The crystallographic $(0\bar{1}11)$ boundaries are similar to the ones observed in natural quartz and amethyst crystals by Lang & Miuscov (1969), McLaren & Phakey (1969). Phakey (1969) McLaren & Pitkethly (1982) and Lu & Sunagawa (1990). They exhibit a normal fringe contrast in the topographs, which is not the case for the irregular ones, where a complex set of fringes is always visible.

According to the theory developed by Authier (1968), the contrast of a stacking fault comes from the relative displacement between the two parts of the crystal. This induces a phase shift Φ between the wavefields propagating through the plane of the fault, which may be quantitatively measured by comparing the fringes in the images with simulations (Authier & Epelboin, 1977). This phase shift may be expressed as $\Phi = 2\pi\,\mathbf{h}\cdot\mathbf{R} \pm (\Phi_R - \Phi_L)$, where $\mathbf{h}$ is the diffraction vector, $\mathbf{R}$ the displacement between the two parts of the crystal and $\Phi_R - \Phi_L$ the phase difference between the structure factors in the two parts of the crystal. The magnitude of $\mathbf{R}$ may be measured by determining the diffraction conditions where the contrast vanishes. The orientation of this displacement may be found by the analysis of the color, black or white, of the first fringe along the exit surface in a section topograph.

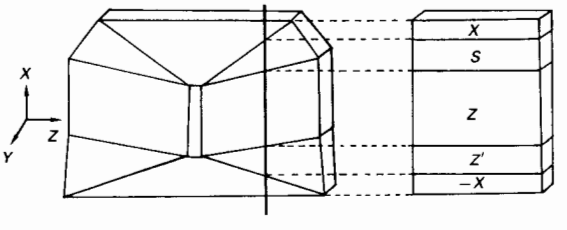

Fig. 1. Geometry of the growth sectors and subsectors. *Y* and *Z* plates.

0021-8898/93/010122-06$06.00

However, this does not apply to the $(0\bar{1}11)$ twin boundary: it is possible to find extinction conditions for the Z' growth sector but not for $-X$. It has been possible, through the study of the Z' growth sector, to estimate the magnitude of **R** as $\pm 1/9$ [100] (González-Mañas & Caballero, 1990). This is in agreement with a previous theoretical study of McLaren & Phakey (1969). Nevertheless, this is not completely satisfactory; the section topographs exhibit very complex fringe patterns, even in the Z' growth sectors where extinction conditions could be found. Extinction conditions for the traverse topographs may also be explained by the geometry of the fault, thus no satisfactory explanation has been given for the structure of the twin boundary.

The aim of this paper is to explain how it has been possible, by means of simulations, to understand the origin of the strange contrast observed in the topographs. It shows that the fault vector is different from the apparent one found in the experiments.

2. Experimental

The geometry of the $(0\bar{1}11)$ twin boundary for the $\bar{2}110$, $20\bar{2}0$, $0\bar{2}20$ and $\bar{3}301$ reflections is shown in Fig. 2. The section topographs have been recorded in the part of the $(0\bar{1}11)$ twin boundary located in the Z' growth sector. Those corresponding to the $\bar{2}110$, $20\bar{2}0$ and $0\bar{2}20$ reflections have been recorded in the same Z plate. The $\bar{3}301$ reflection has been recorded in a Y plate. The thicknesses of the plates were the same. The width of the incident beam was about 20 μm. The values of the structure factors F_h, the components of the dielectric susceptibility χ_h, the extinction distance ξ_h and the phase shift between the structure factors $\Phi_R - \Phi_L$ are given in Table 1.

3. Simulations and discussion

3.1. *Model for the twin boundary*

The simulated X-ray section topographs of the twin boundaries are computed using the program *EMPV* (Epelboin, 1987), which is based on a direct integration of the Takagi–Taupin equations (Epelboin, 1983). Thus there is no approximation as in the theory developed by Authier (1968), where the stationary-phase method had to be used to obtain analytical equations.

Figs. 3(*a*) and (*b*) are typical images of twin boundaries inclined along the exit surface of the crystal. They show the typical 'hour glass' fringes as described by Authier (1968). However, something very unusual must be noticed: the linear absorption is low ($\mu t = 0.76$), thus two kinds of fringes should be visible; the ones corresponding to interference between the newly created wavefields and the normal ones, corresponding to the term I_3 as explained by Authier,

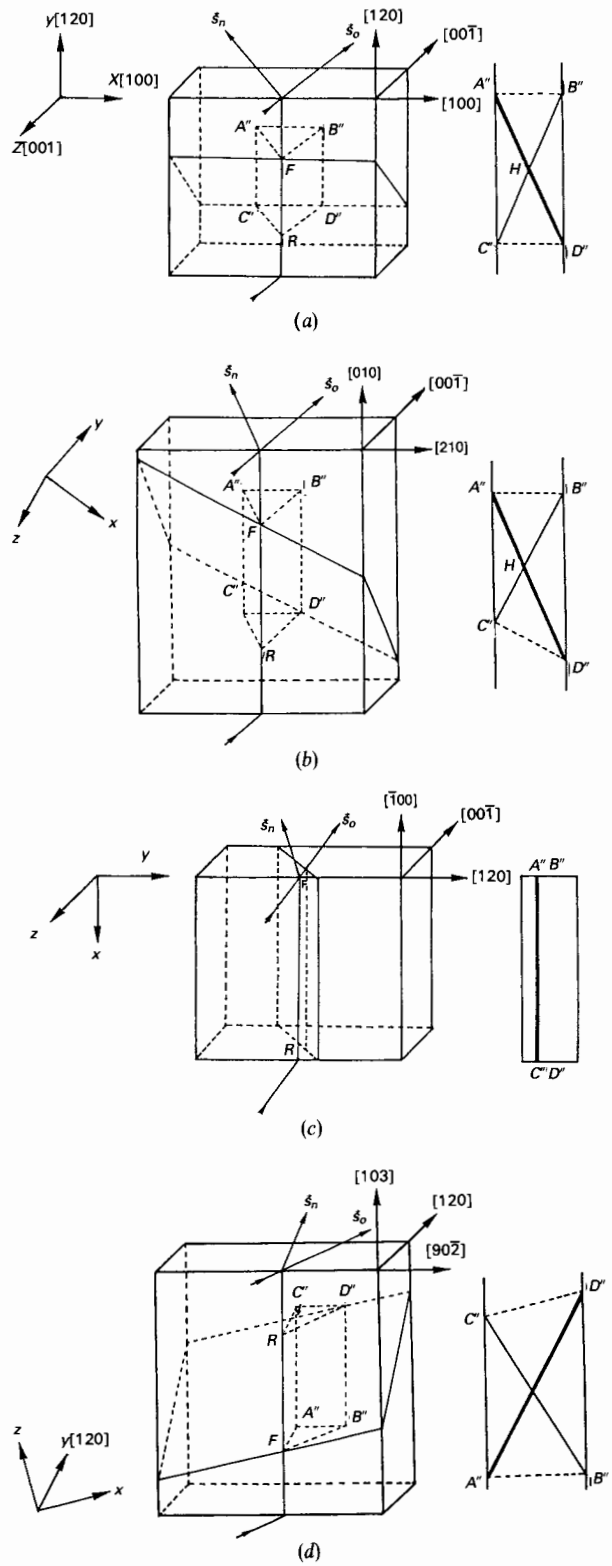

Fig. 2. Geometry of the section topographs. $A''B''$ is the image of the fault near the entrance surface, $C''D''$ is the image near the exit surface and $A''D''$ is the direct image of the fault. (*a*) $\bar{2}110$, (*b*) $20\bar{2}0$, (*c*) $0\bar{2}20$ (*d*) $\bar{3}301$.

and the ones corresponding to interference between the newly created wavefields, corresponding to the term I_2. The interfringe distance which corresponds to I_2 is the extinction distance ξ_h and the interfringe distance for the I_3 fringes is twice that for the I_2 fringes. Thus, the number of visible I_3 fringes in t/ξ_h and the number of I_2 fringes is $2t/\xi_h$, t being the crystal thickness. When absorption increases, the I_2 fringes vanish. The number of fringes exhibited by Figs. 3(*a*) and (*b*) is the one for the I_3 fringes only! Thus, the $(0\bar{1}11)$ twin boundary cannot be described as a simple planar defect.

Fig. 4 shows the simulation of the $(0\bar{1}11)$ twin boundary, computed for different values of the phase shift and for one single planar fault. $\Phi = \Phi_R - \Phi_L$ for the $\bar{2}110$ reflection in Fig 4(*a*), $\pi/6$ in Fig. 4(*b*) and $\pi/9$ in Fig. 4(*c*). Since the linear absorption is low, only I_2 fringes are visible. Their number is twice the number of visible fringes in the experiments shown in Figs. 3(*a*) and (*b*). When the phase shift is changed, neither their number nor their shape is modified. Only their visibility is changed. This is in agreement with the theory and demonstrates that the $(0\bar{1}11)$ twin boundary cannot be described as a simple planar fault.

The observation of the topographs suggests that the twin contrast arises from two parallel planar faults. Thus, we have used the following model in order to compute the simulations of the twin boundaries: a first fault introduces a phase shift Φ_1 and a second fault, parallel to the first one, introduces a phase shift Φ_2. In between, the values of the Fourier components of the dielectric susceptibility are drastically reduced. It means that the walls may be described as lamellae of a poorly diffracting material. If this comes from a lattice misorientation within the walls it is not visible in any topograph but it does not induce any deformation inside the bulk, since this would deform the fringes in the image. This is a model which describes the lamella from the point of view of diffraction for the simulation only and not its structure. Simulations allow one to verify the validity of a given model but do not permit one to determine it when it is unknown.

The total phase shift, through this complex fault, is $\Phi = \Phi_1 + \Phi_2$. The wavefields, when propagating inside the crystal, encounter three parts in the crystal called I, II and III. II is the lamella of thickness a. The

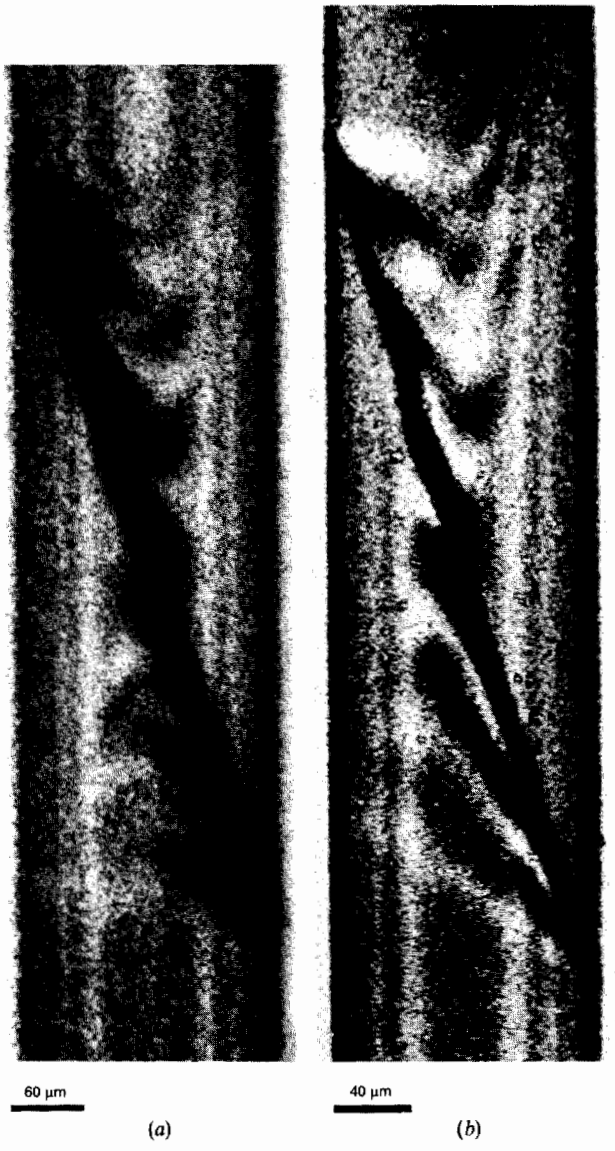

Fig. 3. Image of a $(0\bar{1}11)$ twin boundary in the Z' growth sector. (*a*) Mo $K\alpha$, $\bar{2}110$ reflection. (*b*) Mo $K\alpha$ $20\bar{2}0$ reflection.

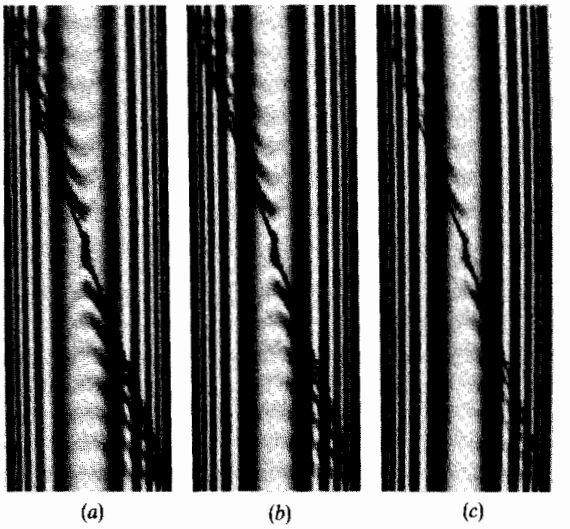

Fig. 4. Simulated images of a single planar defect with the same geometry as the $(0\bar{1}11)$ twin boundary. Diffraction conditions as in Fig. 3. (*a*) $\Phi = \Phi_R - \Phi_L$, (*b*) $\Phi = \pi/6$, (*c*) $\Phi = \pi/9$.

χ_h in the three parts are related as follows:

$$\chi_h^{II} = (1/n)\chi_h^{I} \exp(i\Phi_1),$$

$$\chi_h^{III} = n\chi_h^{II} \exp(i\Phi_2) = \chi_h^{I} \exp[i(\Phi_1 + \Phi_2)],$$

$$\Phi = \Phi_1 + \Phi_2 \text{ now includes } \Phi_R - \Phi_L,$$

where n is an integer number introduced to change the values of the Fourier components of the dielectric susceptibility inside the lamella. Thus, for a given geometry, the contrast of the interference pattern corresponding to the twin boundary is a function of a, n, Φ_1 and Φ_2. By changing these parameters, it is possible to find the best fit between the experiment and simulations.

In a first study we assume that $n = 1$, which means that the boundary is a thick wall of diffracting material. Fig. 5 shows the simulation for $\Phi_1 = \Phi_2 = \pi/9$ for different thicknesses of the boundary. The simulated images are quite similar to those of a simple planar fault. The only effect of the changed thickness of the wall is on the visibility of the fringes. Next, we assume that the Brazil twin boundary is a lamella of non-diffracting material. The results are shown in Fig. 6. As may be noticed by comparison with the experiment shown in Fig. 3(*a*), a change in the phase shift changes the intensity of the fringes as well as their number and shape. The images of Figs. 6(*a*) and (*b*) resemble the experimental one.

Other simulations show that the interference pattern is the same for opposite signs of the phase shift and that the limit value which is visible in the simulations corresponds to a change of $\pi/18$ in Φ_1 and Φ_2. Simulations have been computed in order to adjust the thickness of the non-diffracting lamella and the Fourier components of its dielectric susceptibility. A change in n from 8 to 15 does not modify significantly the contrast. When the thickness of the double fault changes from 10 to 25 μm, the corresponding change in the contrast is too drastic: 10 μm is too small to modify the fringes, 25 μm is too large when one compares the simulated image with the experiment of Fig. 3. Thus we have estimated that the thickness of the twin boundary is of the order of 15 μm. n is of the order of 10, thus χ_h is of the order of 10^{-8} inside the boundary.

The simulations of the Brazil twin diffraction patterns for other reflections confirm these results. Fig. 7 shows images corresponding to the $20\bar{2}0$ reflection, where $\Phi_R - \Phi_L = 0$.

3.2. *Contrast of the* $(0\bar{1}11)$ *boundary*

Next it was necessary to understand why the $(0\bar{1}11)$ Brazil twin boundary presents a different contrast in the traverse topographs, depending on the growth sector. It must be recalled that the contrast may be extinguished for the part of the twin which lies in the Z' growth sector for reflections in zone with the X axis, such as the $\bar{3}301$ reflection. This is not true when the boundary lies in the $-X$ growth sector. This may be understood from the study of the corresponding section topographs: if the traverse topographs are not the same it means that the fringe contrasts of the section topographs differ. The experimental images are shown in Fig. 8. In Fig. 8(*a*), a strong dark line appears, parallel to the edges of the topograph. It corresponds to the direct image of the twin and this shape may be explained by the geometry of the fault

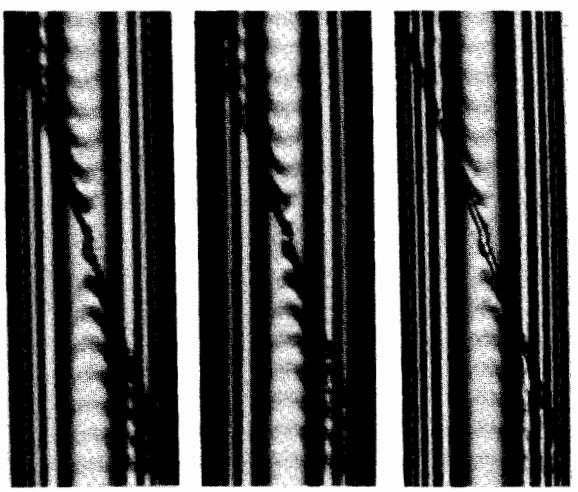

(*a*) (*b*) (*c*)

Fig. 5. Simulated images for the model of the double fault. Diffraction conditions as in Fig. 3. $\Phi = 2\pi/9$. Study of the influence of the thickness of a diffracting boundary ($n = 1$). (*a*) $a = 4$ μm, (*b*) $a = 12$ μm, (*c*) $a = 15$ μm.

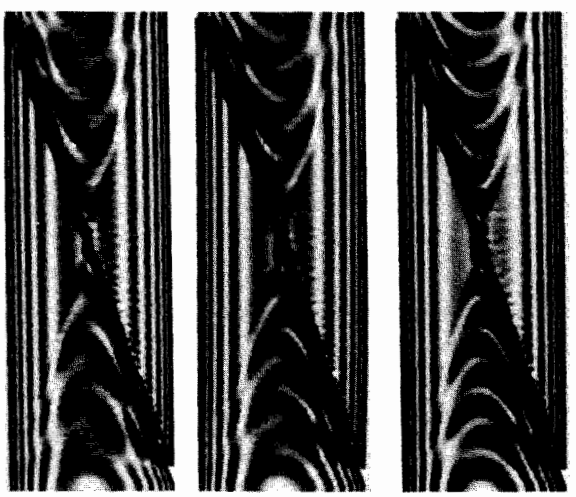

(*a*) (*b*) (*c*)

Fig. 6. Simulated images for the model of the double fault filled with a nondiffracting material ($n = 10$). $a = 15$μm. Diffraction conditions as in Fig. 3. (*a*) $\Phi_1 = \Phi_2 = \pi/9$, (*b*) $\Phi_1 = \Phi_2 = 2\pi/9$, (*c*) $\Phi_1 = \Phi_2 = \pi/3$.

Table 1. *Diffraction parameters for the study*: A_h *and* B_h *are the real and imaginary parts of* F_h, χ_{rh} *and* χ_{ih} ($\times 10^{-7}$) *are the real and imaginary parts of* χ_h *and* $\Phi_R - \Phi_L$ *is the phase shift through the twin boundary*

Values of ξ_h are in μm.

Reflection	$\lvert F_h \rvert$	A_h	B_h	χ_{rh}	χ_{ih}	ξ_h	$\Phi_R - \Phi_L$
$\bar{2}110$	18.1	−17.08	−6.06	6.82	2.42	97.1	$2\pi/9$
$20\bar{2}0$	18.4	18.41	0.0	−7.35	0.0	95.2	0
$\bar{3}301$	30.9	−15.43	−26.72	6.16	10.67	48.1	$2\pi/3$

(see Fig. 2*c*). On the left side of the image, the *Pendellösung* fringes appearing in the Z' growth sector are deformed. One may also notice that the contrast is not the same in the $-X$ and Z' growth sectors. We suggest that these differences are due to the presence of microinclusions associated with the growth bands. In Fig. 8(*b*), a faint complex system of fringes is visible, which disappears in the corresponding traverse topograph since it is the integration of the section topograph.

Using the same data, we have also computed the images for the $0\bar{2}20$ reflection. They confirm our model. Thus we may conclude that the $(0\bar{1}11)$ Brazil twin boundaries may not be described as simple planar defects such as stacking faults. They may be

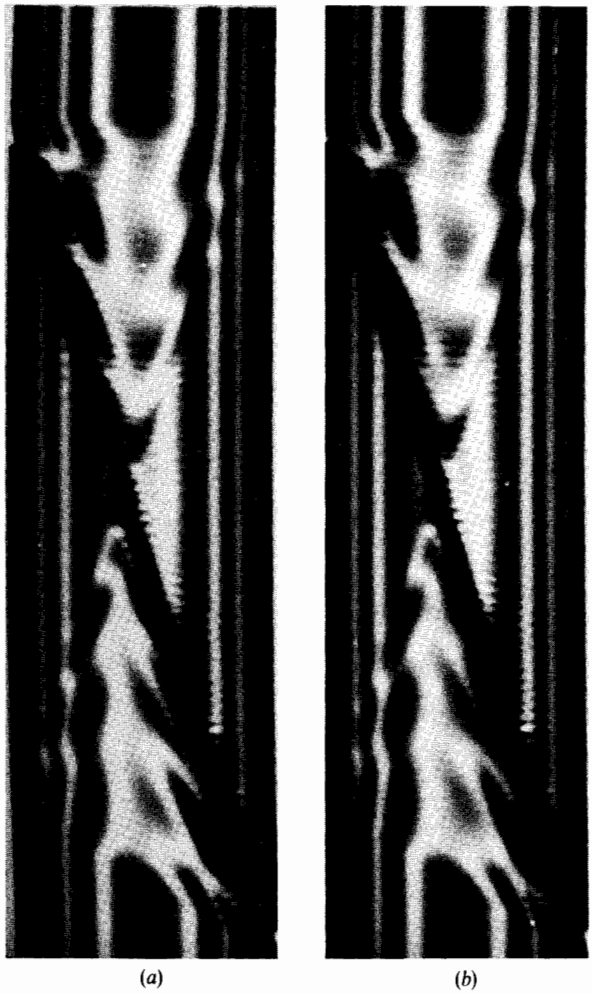

(*a*) (*b*)

Fig 7. Simulation of $(0\bar{1}11)$ boundary. Mo $K\alpha$, $20\bar{2}0$ reflection. (*a*) $\Phi_1 + \Phi_2 = 0$, (*b*) $\Phi_1 + \Phi_2 = \pi/9$.

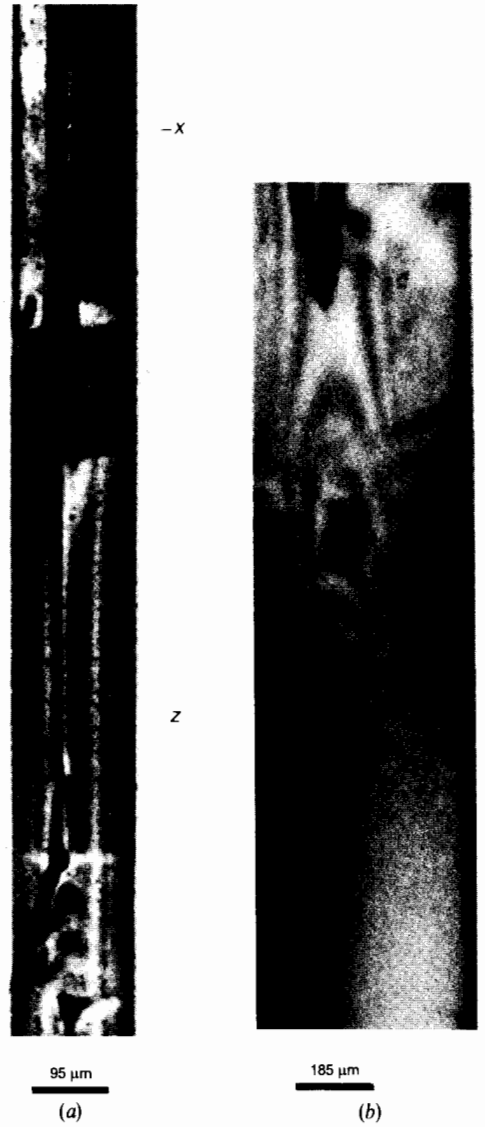

(*a*) (*b*)

Fig. 8. Images of the $(0\bar{1}11)$ Brazil twin boundary in the Z' growth sector Mo $K\alpha$. (*a*) $0\bar{2}20$ reflection, (*b*) $\bar{3}301$ reflection.

described as thick lamellae which contain non-diffracting material. This is confirmed by optical observation with a microscope: the $(0\bar{1}11)$ Brazil twin boundaries are visible all along the surface of the polyhedra which appear in the $-X$ faces. Their thickness is of the same order of magnitude as the one determined in the simulations.

It is not possible to determine which kind of deformation is responsible for the non-diffracting material inside the boundaries. The resolution of the topograph is limited and this limitation may not be solved by means of simulations. If this is due to a distribution of dislocations, González-Mañas & Caballero (1991) have shown that its density must be fairly low.

The visibility of the fringes permits one to say that there does not exist an important strain gradient associated with a high concentration of impurities, at least in the $(0\bar{1}11)$ twin boundaries located in the Z' growth sectors.

Transmission electron microscopy will be necessary for a more detailed study of these problems.

Concluding remarks

We have shown that Brazil twin boundaries in Y-bar synthetically grown quartz crystals may be modelled as lamellae of nondiffracting materials. In section topographs, they exhibit fringes which are sensitive to the thickness of the lamellae. It has been possible to evaluate this thickness as being of the order of 15 μm for $(0\bar{1}11)$ twin boundaries. The boundary may be described as a poorly diffracting material which may be simulated by reducing the Fourier components of the dielectric susceptibility by a factor of ten within the boundary. It does not induce any deformation inside the bulk and there is no evidence that it is due to a lattice misorientation since this should diffract in some experiments. However the simulation does not allow one to determine if the boundary introduces a phase shift smaller than $\pi/9$.

This study has been supported by a grant from CYCIT PB87-967. The crystals were provided by SICN, Annecy, France.

References

AUTHIER, A. (1968). *Phys. Status Solidi*, **27**, 77–93.
AUTHIER, A. & EPELBOIN, Y. (1977). *Phys. Status Solidi A*, **41**, K9–K14.
EPELBOIN, Y. (1983). *Acta Cryst.* A**39**, 761–767.
EPELBOIN, Y. (1987). *Prog. Cryst. Growth Characteriz. Mater.* **14**, 465–506.
GONZÁLEZ-MAÑAS, M. & CABALLERO, M. A. (1990). *Bol. Soc. Esp. Miner.* **13**, 19–24.
GONZÁLEZ-MAÑAS, M. & CABALLERO, M. A. (1991). *J. Cryst. Growth*, **13**, 669–680.
LANG, A. R. & MIUSCOV, V. F. (1969). *Growth Cryst. (USSR)*, **7**, 112–123.
LU, T. & SUNAGAWA, I. (1990). *J. Cryst. Growth*, **99**, 1232–1237.
MCLAREN, A. C. & PHAKEY, P. P. (1969). *Phys. Status Solidi*, **31**, 723–737.
MCLAREN, A. C. & PITKETHLY, D. R. (1982). *Phys. Chem. Miner.* **8**, 128–135.
PHAKEY, P. P. (1969). *Phys. Status Solidi*, **34**, 105–119.